Journal of Materials Chemistry B

RSC Publishing

PAPER

View Article Online
View Journal | View Issue

Cite this: *J. Mater. Chem. B*, 2013, **1**, 186

Growth of gold nanowires on flexible substrate for highly sensitive biosensing: detection of thrombin as an example†

Yu-Liang Chen,[a] Chi-Young Lee[b] and Hsin-Tien Chiu*[a]

Received 23rd August 2012
Accepted 1st October 2012

DOI: 10.1039/c2tb00010e

www.rsc.org/MaterialsB

We demonstrated a facile fabrication of high density Au nanostructures including nanothorns (NTs), nanocorals (NCs), nanoslices (NSs), and nanowires (NWs) which were electrochemically grown on flexible plastic substrates of polyethylene terephthalate (PET). A thrombin-binding aptamer was immobilized on the surfaces of the Au nanostructures to form highly sensitive electrochemical impedance spectroscopic (EIS) biosensors for thrombin recognition. The binding of thrombin to the aptamer sequence was monitored by EIS in the presence of $[Fe(CN)_6]^{3-/4-}_{(aq)}$. The protein (1–50 pM) was detected linearly by the Au nanostructures. Among them, the Au NWs exhibited excellent thrombin detection performances. The biosensor provided high sensitivity, selectivity, and stability due to its high surface area.

Introduction

Electrochemical sensors have been widely utilized in many clinical, food, environmental, and defense applications due to their high performances in sensitivity, rapidity, easy usage, and low-cost.[1,2] Based on different electrochemical reactions, many devices have been developed as amperometric, potentiometric, field-effect, and impedance sensors.[3,4] Among them, impedance sensors for electrochemical impedance spectroscopy (EIS) have shown effective measurement for many analytes due to their sensitive nature towards minute variations between the electrode/electrolyte interfaces.[5–8] This feature is usable for heavy metal ion, DNA, protein, and bacteria detection. For sensing analytes selectively by EIS, the sensing electrodes are commonly modified with high target-binding recognition units. Antibody–antigen, enzyme–biomolecule, and aptamer–protein pairs are regularly involved.[9–12] For sensing proteins, corresponding aptamers present significant advantages over other recognition elements. Generally, aptamers are low molecular weight, easily synthesized and immobilized, and with good stability and reproducibility. As a result, applying aptamers as recognition elements in electrochemical biosensors has been widely developed.[13,14] In these applications, nano-sized materials, such as carbon nanotubes (CNTs) and metal nanoparticles (NPs), are commonly fabricated on substrates to serve as working electrodes. These sensors enhance electrochemical signal responses of the analytes due to their high surface area, good stability, and excellent conductivity.[15–18] Previously, we demonstrated facile electrochemical depositions of various Au nanostructures on carbon, silicon, and glass substrates.[19–21] In this study, we wish to report the simple electrochemical growth of several Au nanostructures, including Au nanothorns (NTs), Au nanocorals (NCs), Au nanoslices (NSs), and Au nanowires (NWs), on flexible commercial transparencies made from polyethylene terephthalate (PET). The nanostructures, especially the high aspect ratio one-dimensional NWs, provide greatly increased surface areas. This feature is extremely important for electrochemical biosensing applications. To explore their potential as highly sensitive EIS electrodes, we selected the thrombin aptamer–thrombin system as the biosensing platform. Thrombin is an important regulator for blood coagulation reactions. Normally, thrombin is not present in the blood stream. However, in certain diseases, the protein can reach low-picomolar concentrations in a patient's blood.[22] Thus, the presence of a trace of thrombin would lead to blood clot formation. By immobilizing thrombin aptamer on the Au NWs on the PET substrates, we have successfully developed flexible EIS electrodes for selective thrombin sensing in the picomolar range.

Experimental section

Chemicals and instruments

$HAuCl_4 \cdot 3H_2O$ (99%), $Na_2HPO_4 \cdot 2H_2O$ (99.5%), $HS(CH_2)_6OH$ (MCH, 97%), $(HOCH_2)_3CNH_2 \cdot HCl$ (Tris–HCl, 97%), $K_4Fe(CN)_6 \cdot 3H_2O$ (99.9%), human α-thrombin (≥2000 NIH units per mg protein), bovine serum albumin (BSA, 96%), and avidin

[a]*Department of Applied Chemistry, National Chiao Tung University, 1001, University Rd, Hsinchu, Taiwan, R. O. C. E-mail: htchiu@faculty.nctu.edu.tw*

[b]*Department of Materials Science and Engineering, National Tsing Hua University, 101, Sec. 2, Kuang-Fu Road, Hsinchu, Taiwan, R. O. C. E-mail: cylee@mx.nthu.edu.tw*

† Electronic supplementary information (ESI) available. See DOI: 10.1039/c2tb00010e

(98%) were purchased from Sigma-Aldrich. $P(CH_2CH_2–COOH)_3 \cdot HCl$ (TCEP, 98%), $K_3Fe(CN)_6$ (98%), and $[Ru(NH_3)_6]Cl_3$ (RuHex, Ru 32.1% min) were supplied by Alfa Aesar. $MgCl_2$ (98%) was provided by Showa. NaH_2PO_4 (99.6%), NaCl (99%), and KCl (99.6%) were obtained from J. T. Baker. Cetyltrimethylammonium chloride (CTAC, 890 mM) was contributed by Taiwan Surfactant. $NaNO_3$ was purchased from Riedel-de Haën. Thrombin-binding aptamer I (TBAI, 5′-SH-$(CH_2)_6$-GGT TGG TGT GGT TGG-3′, 10 OD) was supplied by BioTD. Aqueous solutions were prepared in deionized water (DI water, MilliQ, 18 MΩ). All experiments were performed at room temperature.

SEM images and EDS data were obtained from a JEOL JSM-7401F (15 keV). TEM images and SAED patterns were taken from a JEOL JEM-3000F (300 kV). Thin films were grown by using an e-gun evaporation system AST PEVA 600I. Electrochemical deposition experiments were performed with a DC power supply GW Instek GPS-1830D. Cyclic voltammetry (CV), chronocoulometry (CC), and electrochemical impedance spectroscopy (EIS) measurements were performed with a CHI 6081C electrochemical workstation.

Fabrication of nanostructured Au on flexible substrates

Thin layers of Ti (20 nm) and Au (80 nm) were evaporated sequentially on to a PET transparency to form a flexible conductive substrate. An electrodeposition solution composed of $HAuCl_{4(aq)}$, $CTAC_{(aq)}$ and $NaNO_{3(aq)}$ was prepared in DI water (see Table 1). At a controlled temperature, Au nanostructures were grown on the flexible substrate (cathode) at a controlled voltage by using the two-electrode electrochemical deposition system shown in Fig. S2 in the ESI.† A carbon electrode was used as the anode. After 24 h, the flexible electrode was isolated, rinsed with alcohol and DI water, and then dried with a flowing stream of $N_{2(g)}$.

Modification of nanostructured Au on flexible substrates by TBAI and MCH

A TBAI solution was prepared before the Au surface was modified. In a binding buffer (BB, pH 7.4) composed of Tris–$HCl_{(aq)}$ (50 mM), $NaCl_{(aq)}$ (100 mM), $MgCl_{2(aq)}$ (10 mM) and $KCl_{(aq)}$ (100 mM), a solution of TCEP (10 mM) and TBAI (5 μM) was prepared. The solution was heated to 368 K for 5 min and cooled to room temperature for G-quadruplex formation. Then, a nanostructured Au substrate was immersed in the solution (1 mL) at room temperature for 24 h. After washing with DI water, the substrate was dipped in MCH (1 mM in BB) at room temperature for 2 h. Finally, the sample was rinsed with DI water and dried under $N_{2(g)}$.

Electrochemical analyses of nanostructured Au on flexible substrates

A conventional three-electrode system was employed for all electrochemical analyses. The working electrode was a nanostructured Au electrode (0.5 cm × 0.5 cm) fabricated in this study while the counter and the reference were a Pt wire and an Ag/AgCl electrode, respectively. CV experiments (−0.2 to 1.6 V at 50 mV s^{-1}) were carried out in $H_2SO_{4(aq)}$ (0.5 M) to measure the real surface area (RSA) of the electrode. CC experiments (−0.4 to 0.2 V at pulse period 0.5 s) in $[Ru(NH_3)_6]Cl_{3(aq)}$ (1 mM) were employed to determine the immobilized density of TBAI on the Au substrate. The TBAI/MCH-modified Au substrate was immersed a thrombin solution (1–50 pM) at room temperature for 30 min before measurements. All EIS experiments (0.1 to 10^5 Hz, 5 mV) were carried out in the PBS solution containing $Fe(CN)_6^{3-}/Fe(CN)_{6(aq)}^{4-}$ (1 : 1, 2.5 mM).

Results and discussion

Fabrication and characterization of Au nanostructures on flexible substrates

On flexible commercial PET transparencies, a Ti adhesion layer (thickness: 20 nm) and an Au seeding layer (for further Au nucleation, thickness: 80 nm, Fig. S1 in the ESI†) were grown by using an e-gun evaporation system. Bending the substrate is displayed in Fig. 1a, revealing its flexible nature. Au

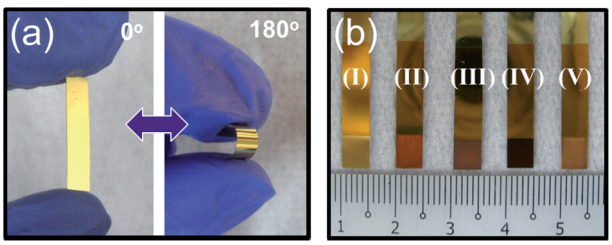

Fig. 1 Images of (a) a flexible substrate with an Au/Ti/PET structure and (b) substrates after the growth of Au nanostructures (bottom, 0.5 × 0.5 cm^2; (I) film, (II) NTs, (III) NCs, (IV) NSs, and (V) NWs).

Table 1 Fabrication conditions and electrochemical properties of nanostructured Au electrodes

Structure	Electrodeposition[a]			Au weight (μg)	RSA (cm^2)	Specific RSA (cm^2 g^{-1})	Total amount of TBAI (molecules)	Thrombin detection sensitivity (Ω pM^{-1} cm^{-2})	R^2
	CTAC[b] (mM)	Voltage (V)	Temp (K)						
Film	—	—	—	—	0.180	—	1.32×10^{13}	79.2	0.989
NTs	5.0	0.70	288	161	0.530	3300	1.77×10^{13}	360	0.983
NCs	10.0	1.60	288	201	1.21	6010	2.90×10^{13}	460	0.988
NSs	10.0	1.00	288	165	1.01	6120	3.30×10^{13}	604	0.994
NWs	10.0	0.70	298	84.6	2.21	26 100	5.88×10^{13}	1130	0.995

[a] Growth time: 24 h. Geometric area of substrate: 0.25 cm^2. [b] In $HAuCl_{4(aq)}$ (5 mM) and $NaNO_{3(aq)}$ (20 mM).

nanostructures were deposited on the flexible substrates (0.5 cm × 0.5 cm) by reducing $HAuCl_{4(aq)}$ in a two-electrode electrochemical deposition system as shown in Fig. S2.† The flexible substrate was employed as the cathode while a carbon electrode was used as the anode. The electrolyte was a solution containing $HAuCl_{4(aq)}$, $NaNO_{3(aq)}$, and cetyltrimethylammonium chloride (CTAC). By controlling the reaction parameters, such as CTAC concentration, applied voltage, and temperature shown in Table 1, Au nanostructures, including nanothorns (NTs), nanocorals (NCs), nanoslices (NSs), and nanowires (NWs) were electrochemically grown on the flexible PET substrates. Characterization of the nanostructures will be discussed below. Appearances of the flexible substrates after the nanostructure depositions are displayed in Fig. 1b.

The as-obtained samples were investigated by scanning electron microscopy (SEM), transmission electron microscopy (TEM), and energy dispersive X-ray spectroscopy (EDS). The corresponding results are revealed in Fig. 2a–d, e–h, and S3 in the ESI.† The EDS data confirm that all of the solids deposited on the flexible substrates are pure Au. The SEM image in Fig. 2a reveals a complete coverage of NTs on the substrate. They have a height of 0.2–1 μm, a basal side width of 100–200 nm, and a tip width of 20–50 nm. The thickness of the deposited Au NT layer on the substrate is about 4 μm (Fig. S4a in the ESI†). The TEM image in Fig. 2e reveals the dimensions of a representative NT. It has a height of 200 nm, a projected basal width of 100 nm, and a tip width of 20 nm. From the selected area electron diffraction (SAED) pattern shown in the inset of Fig. 2e, the NT is determined to be a faced-centered cubic (fcc) single crystal. The lattice parameter a is estimated to be 0.41 nm, in good agreement with the literature value of Au, 0.408 nm (JCPDS-04-0784). The pattern is indexed to the [011] zone axis and the [1$\bar{1}$1] growth direction for the NT. The SEM image in Fig. 2b shows that irregular coral-like structures with a width of about 100 nm were grown on the flexible PET substrate. In Fig. S4b,† the layer thickness of the NC is measured to be 4 μm. A fragment of NC is observed by TEM in Fig. 2f. The quasi-one-dimensional structure is composed of major stems and branches. Its SAED pattern, shown in the inset of Fig. 2f, also agrees with that of the single crystalline fcc structure of Au. From the pattern, the [112] zone axis is indexed and the [110] growth direction is determined for the observed NC. In addition, the lattice parameter is calculated to be 0.41 nm. The SEM image of NSs is displayed in Fig. 2c. It reveals that each thin slice has a thickness of 10–20 nm and a width of 0.2–1 μm. The side-view image shown in Fig. S4c† displays a thickness of about 7 μm for the NS layer. The TEM image in Fig. 2g reveals the structure of a representative NS. It has a smooth surface and a size of about 400 nm. The SAED pattern (Fig. 2g, inset) shows that, in addition to the bright spots from an fcc single crystal, faint spots are observed. After the [$\bar{1}$11] zone axis is indexed for the NS, the bright allowed {220} spots and the faint forbidden 1/3 {422} spots are indexed as well. The observed forbidden spots are due to the presence of two-plane twin planes, which are parallel to each other, in the NS.[23] From the pattern, the lattice parameter is estimated to be 0.41 nm. High-aspect ratio NWs, which cover the flexible substrate densely, are shown in the SEM image in Fig. 2d. Each of the NWs has a diameter of 20–100 nm and a length of 10–20 μm. As shown in Fig. S4d,† the NW layer is much thicker than the other layers although the deposited weight is significantly lower than the others. Presumably, the NWs grow more in a unidirectional way. The TEM image in Fig. 2h reveals a representative NW with a diameter of 50 nm. The SAED pattern in the inset of Fig. 2h is also the result of an fcc single crystal. From the pattern, the [011] zone axis is indexed while the NW growth is determined to be along the [1$\bar{1}$1] direction. The lattice parameter is calculated to be 0.41 nm, which agrees with the reported value of Au.

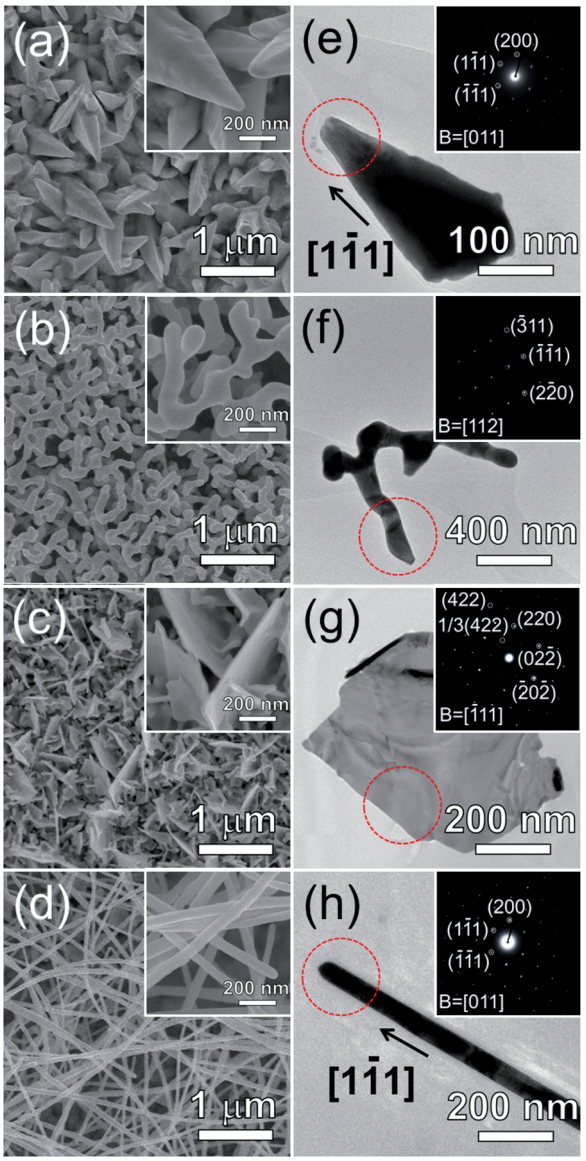

Fig. 2 Low and high magnification (insets) SEM images of Au nanostructures on flexible PET substrates: (a) NTs, (b) NCs, (c) NSs, and (d) NWs. TEM images and SAED patterns (insets, from the circled regions) of Au nanostructures: (e) NTs, (f) NCs, (g) NSs, and (h) NWs.

Growth scheme of Au nanostructures

We suggest the following pathway, as shown in Scheme 1, to illustrate the observed Au nanostructure growth. Fabrication of

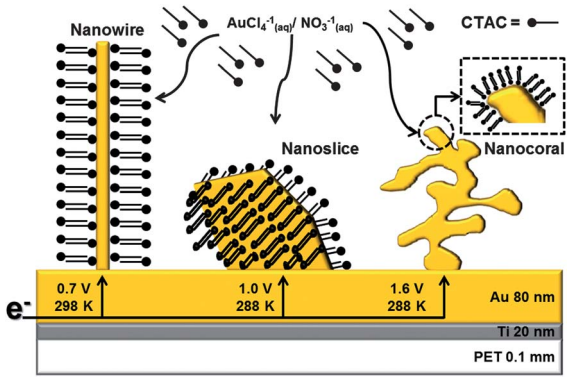

Scheme 1 Proposed growth mechanism of Au nanostructures on a flexible substrate.

the Au/Ti layers on the flexible PET substrate was essential for the later seeding of the electrochemical deposition of the Au nanostructures. Previous investigations indicated that the presence of an appropriate quantity of surfactant molecules in electrodeposition could influence the product morphology significantly.[19–21] CTAC molecules acted as the capping agent on as-formed Au surfaces and reduced their surface energies.[24–26] We speculate that the surfactant molecules might adsorb selectively on low-index facets, such as Au {100} and {110} surface planes, to inhibit the Au growth in these directions. Additionally, the morphology was altered by adding an appropriate quantity of $NaNO_{3(aq)}$. Its presence not only increased the solution conductivity but also removed unstable surface sites.[27] The applied voltage affected the product morphology too. One-dimensional Au NWs and NTs were obtained at a carefully controlled low voltage. The combination of the low voltage and the surfactant inhibited Au nucleation and growth on specific sites. The slow Au deposition also facilitated the anisotropic growth. On the other hand, the anisotropic growth was less controlled at high applied voltages. As a result, Au NSs and NCs were obtained. For Au NWs, the applied growth temperatures were slightly higher than the ones used for the other Au nanostructures so that the NWs could be grown at reasonable rates.

Real surface areas of Au nanostructures

The real surface areas (RSAs) of various nanostructured Au substrates were measured in $H_2SO_{4(aq)}$ by cyclic voltammetry (CV). The CV diagrams in Fig. S5† display the oxidation and reduction of a monolayer of Au on the corresponding nanostructures. The initial anodic currents starting at about 1.0 V in the positive potential scans are due to the formation of Au oxides. Subsequently, the surface oxides are reduced at about 0.9 V in the negative scans. By integrating the reduction currents, the RSAs of the nanostructures are calculated. It is assumed that the reduction of a monolayer of Au oxide requires 390 ± 10 C cm^{-2}.[28] All of the calculated RSAs are listed in Table 1. The electric currents applied to the electrochemical depositions were recorded (Fig. S6 in the ESI†). The data are converted into weights for the deposited Au nanostructures. Specific RSAs in cm^2 g^{-1} are derived and shown in Table 1. Clearly, the specific RSA of the Au NWs, 26126 cm^2 g^{-1}, is the highest one. This is due to the high aspect ratio of the one-dimensional NW structure. This allows more exposed Au atoms on the surface. Thus, we expect the Au NWs could show the best performance in the experiments discussed below.

Modification of nanostructured Au surfaces by thrombin aptamer

In order to determine thrombin selectively, it was necessary that the thrombin-binding aptamer (TBAI) was immobilized on the nanostructured Au surfaces to provide selective thrombin binding ability. The core sequence of TBAI is a 15-mer oligonucleotide 5′-SH-$(CH_2)_6$-GGT TGG TGT GGT TGG-3′. It can bind to the fibrinogen-recognition exosite of thrombin.[29,30] In a binding buffer solution containing cations Na^+, K^+ and Mg^{2+}, TBAI folds into a chair-type G-quadruplex structure which plays an important role in the thrombin binding.[31,32] In Scheme 2, modification steps of the Au surface are shown. Initially, a monolayer of thiolated-TBAI is self-assembled on an Au surface.

Next, for eliminating non-specific adsorptions, unoccupied Au surface sites are further blocked by adsorption of MCH molecules. Then, the TBAI/MCH modified Au substrate is ready to interact selectively with thrombin for subsequent electrochemical analyses.

The chronocoulometric (CC) data shown in Fig. 3a are used to estimate the surface coverages of TBAI on the nanostructured Au electrodes.[33] An electrolyte containing $[Ru(NH_3)_6]^{3+}$ (RuHex) was employed as a cationic redox marker which bound electrostatically to the anionic phosphate groups of TBAI. The electrochemical responses from CC experiments were due to the double-layer charge and the charge generated by RuHex adsorbed on the TBAI/MCH-modified Au surfaces. When the RuHex/TBAI binding was completely saturated, the aptamer coverage density on the Au nanostructures, Γ_{TBAI}, could be calculated by employing the following equations:[33]

$$Q = Q_{dl} + nFA\Gamma_{Ru} \quad (1)$$

$$\Gamma_{TBAI} = \Gamma_{Ru}(z/m)N_A \quad (2)$$

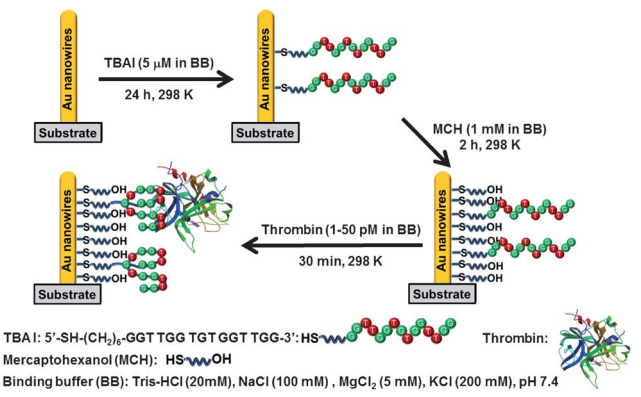

Scheme 2 Surface modifications of Au nanostructures by TBAI and detection of thrombin.

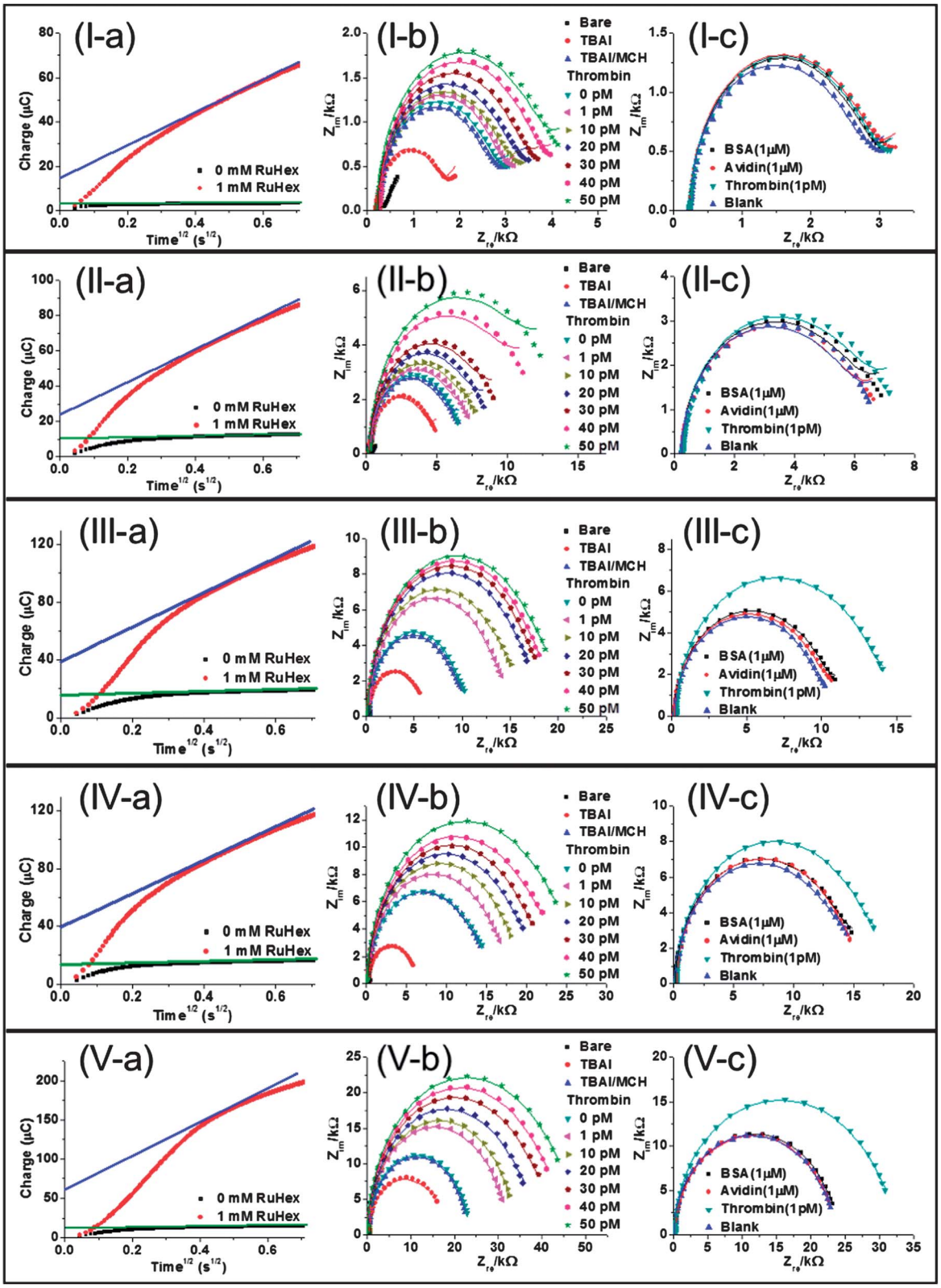

Fig. 3 Electrochemical characterization of Au nanostructures on flexible substrates, I: bare film, II: NTs, III: NCs, IV: NSs, and V: NWs. (a) Chronocoulometric responses of TBAI/MCH-modified Au nanostructures in the presence (red) and absence (black) of RuHex (1 mM). From the fitted lines (blue and green), the intercepts at $t = 0$ are determined. (b) Nyquist plots from EIS measurements of various modified-electrode/electrolyte interfaces before and after stepwise adsorption of thrombin on TBAI/MCH modified surfaces. (c) Nyquist plots of TBAI/MCH-modified electrodes, in the presence of black: BSA (1 μM), red: avidin (1 μM), green: thrombin (1 pM), and blue: blank. Curves are fitted from the experimental data displayed.

Here, Q is the capacitive charge of the measured substrate surface, determined from the CC intercept at $t = 0$. Q_{dl} represents the double layer capacitive charge of the original RuHex-free surface. $nFA\Gamma_{Ru}$ stands for the charge required for the reduction of RuHex adsorbed on TBAI (n: number of electrons per molecule for reduction, F: Faraday constant, A: substrate area). Γ_{Ru} corresponds to the adsorbed surface concentration of RuHex while Γ_{TBAI} symbolizes the adsorbed surface density of the aptamer molecules. Parameters z, m and N_A are the charge of RuHex, the number of the bases in TBAI, and Avogadro's number, respectively. From the equations, the total amounts of TBAI covered on the nanostructured Au substrates are evaluated and listed in Table 1. Again, due to the high RSA, the electrode composed of Au NWs shows the maximum total amount of TBAI molecules, 5.88×10^{13}, on the surface. Consequently, we anticipate the electrode of TBAI/MCH-modified Au NWs could bind the greatest amount of thrombin molecules and show the highest electrochemical response signals.

Detection of thrombin *via* electrochemical impedance spectroscopy

The usage of the nanostructured Au flexible substrates for sensing thrombin was measured *via* electrochemical impedance spectroscopy (EIS), which provides important response signals about the electrode/electrolyte interface, which was employed for sensing thrombin by the TBAI/MCH-modified Au nanostructures fabricated in this study.[34–36] $[Fe(CN)_6]^{3-/4-}_{(aq)}$ was used as the redox probe to show the corresponding Nyquist plots (Fig. 3b) from the EIS experiments. The experimental Nyquist plots were fitted with simulated results using the Randle-modified equivalent circuit model shown in Fig. S7.†[37] All of the elementary parameters in the simulations for various nanostructured Au substrates are listed in Tables S1–S5.† Among the parameters, electron transfer resistance (R_{et}) provides important information related to electron transfers of the redox probe molecules near the electrode/electrolyte interface. From the semicircles in the Nyquist plots, R_{et} values were estimated. In Fig. 3b, bare surfaced Au substrates do not exhibit observable semicircles due to very efficient electron transfers between the probe molecules and the surfaces. After subsequent TBAI and MCH modifications of the Au surfaces, the semicircles in the Nyquist plots increase as well. These indicate increased R_{et} between the probe molecules and the Au surfaces due to the surface modifications. After the surface-modified Au electrodes were incubated in increasing concentrations (1–50 pM) of thrombin solutions, the corresponding Nyquist plots exhibit increased semicircles, indicating increased R_{et} values. Variations of R_{et} value differences, ΔR_{et}, against thrombin concentrations are plotted in Fig. 4a. While a linear relationship is observed for each one of the nanostructured Au electrodes with modified surfaces, the one composed of Au NWs reveals the steepest slope. This corresponds to the greatest thrombin detection sensitivity, 1130 Ω pM^{-1} cm^{-2}, among all of the Au electrodes. Clearly, this is a consequence of the high RSA and the high total amount of TBAI molecules found for the Au NWs. In contrast, the Au film electrode shows an extremely small

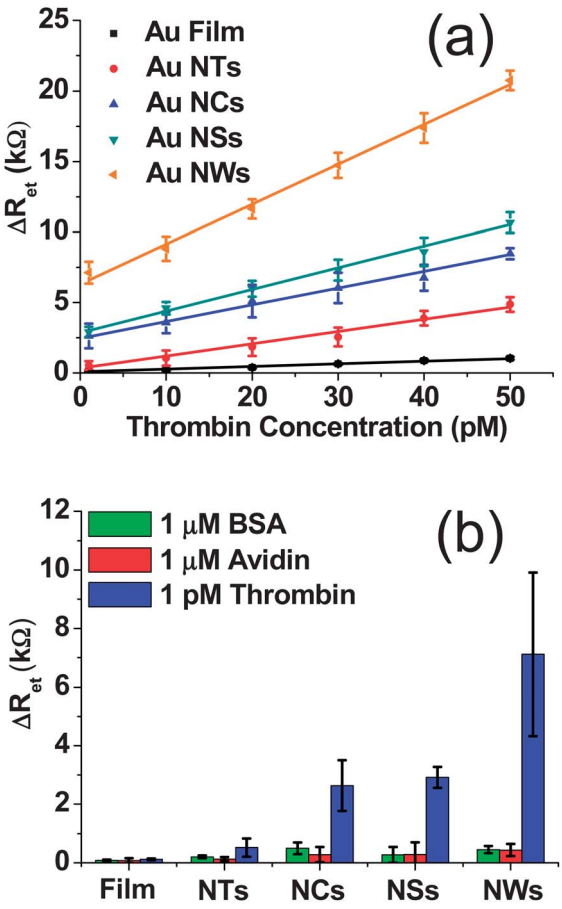

Fig. 4 (a) Calibration curves of ΔR_{et} *versus* concentration of thrombin for TBAI-modified Au nanostructures, black: bare film, red: NTs, blue: NCs, green: NSs, and orange: NWs. The error bars indicate the standard deviation of three successive measurements. (b) Responses of ΔR_{et} to different proteins, green: BSA (1 μM), red: avidin (1 μM), and blue: thrombin (1 pM). Error bars indicate the standard deviations of three successive measurements.

thrombin detection sensitivity, 79.2 Ω pM^{-1} cm^{-2}. All of the sensitivity results are presented in Table 1. In general, the sensitivity increases with increased amount of TBAI molecules adsorbed on the Au electrode.

Selectivity of TBAI/MCH-modified Au electrodes toward other proteins

Selectivity of the TBI/MCH-modified Au electrodes was investigated by EIS. In the presence of other proteins, such as BSA and avidin, their electrochemical responses were measured. Nyquist plots and ΔR_{et} values derived from the experiments involving these proteins are compared with the data from thrombin and presented in Fig. 3c. In relatively high concentration (1 μM) of BSA and avidin solutions, ΔR_{et} values increase only slightly. In contrast, in a low concentration (1 pM) of thrombin solution, all of the nanostructured Au except the film electrode show significant responses. Obviously, the TBAI/MCH-modified Au substrates demonstrate excellent selectivity for sensing thrombin molecules. The results are summarized and displayed in Fig. 4b. Among the electrodes with various Au nanostructures,

Table 2 Summary of reported performances of thrombin detection

Electrodes	Analytical technique[a]	Detection range	LOD[b]	Ref.
Au nanoparticle	CV	1 pM to 30 nM	1 pM	38
SWCNT/Au nanoparticle	DPV	0.02–45 nM	11 pM	39
Au nanoparticle	DPV	12 pM to 1.2 μM	12 pM	40
CNT	EIS	0.39–3.9 nM	105 pM	41
Au nanoparticle	EIS	30 nM	13 pM	42
Au film	EIS	0.12–30 nM	30 pM	43
Au film	EIS	5–35 nM	2 nM	44
Au/polyamidoamine dendrimer	EIS	1–50 nM	10 pM	45
Au film	EIS	10 pM to 100 nM	10 pM	46
Graphite	EIS	7.5–75 pM	4.5 pM	47
Au film	EIS	10–50 pM	0.4 pM	This study
Au NTs	EIS	1–50 pM	0.4 pM	This study
Au NCs	EIS	1–50 pM	0.4 pM	This study
Au NSs	EIS	1–50 pM	0.3 pM	This study
Au NWs	EIS	1–50 pM	0.2 pM	This study

[a] CV: cyclic voltammetry, DPV: differential pulse voltammetry, EIS: electrochemical impedance spectroscopy. [b] LOD: limit of detection, estimated from three times the standard deviation of the experimental data.

the NWs electrode reveals the highest responsive thrombin selectivity. This is attributed to the high RSA and high thrombin sensitivity of the TBAI/MCH-modified Au NWs electrode.

Conclusions

In this study, we have demonstrated that several Au nanostructures, including Au NTs, Au NCs, Au NSs, and Au NWs, can be grow on flexible PET substrates *via* simple electrochemical depositions. The electrode composed of Au NWs reveals the highest RSA, and specific RSA. These are attributed to the unique one-dimensional structure of the NWs, which allows more exposed surface area than the other nanostructures do. Consequently, employing the as-fabricated Au nanostructures for possible biosensing applications has been explored. Thrombin was selected as the target molecule for probing. After the Au surfaces were modified by TBAI, the Au NWs electrode adsorbed the highest total amount of the molecule. In turn, this electrode provided the best thrombin detection sensitivity, selectivity, and linear relationship. In comparison with the thrombin detection performances of other nanomaterials, as summarized in Table 2, our nanostructured Au electrodes are capable of sensing the target molecule in an extremely low concentration at the picomolar level (1–50 pM).[38–47] Especially, the Au NWs on the flexible substrate can perform exceptionally with the lowest limit of detection of thrombin at 0.2 pM. To our knowledge, these are among the best electrochemical thrombin sensors reported in literature. Equipped with this model example, we anticipate that the strategy can be extended to the detection of other biologically important proteins. Utilizing the highly sensitive Au NWs electrode for the explorations is under way.

Acknowledgements

We are grateful for the support from the National Science Council, "Aim for the Top University Plan" of the National Chiao Tung University, and the Ministry of Education of Taiwan, the Republic of China.

Notes and references

1 D. Grieshaber, R. MacKenzie, J. Vörös and E. Reimhult, *Sensors*, 2008, **8**, 1400–1458.
2 N. J. Ronkainen, H. B. Halsall and W. R. Heineman, *Chem. Soc. Rev.*, 2010, **39**, 1747–1763.
3 B. J. Privett, J. H. Shin and M. H. Schoenfisch, *Anal. Chem.*, 2010, **82**, 4723–4741.
4 D. W. Kimmel, G. LeBlanc, M. E. Meschievitz and D. E. Cliffel, *Anal. Chem.*, 2011, **84**, 685–707.
5 R.-G. Cao, B. Zhu, J. Li and D. Xu, *Electrochem. Commun.*, 2009, **11**, 1815–1818.
6 Y. Wang, C. Li, X. Li, Y. Li and H.-B. Kraatz, *Anal. Chem.*, 2008, **80**, 2255–2260.
7 S.-J. Lee, V. Anandan and G. Zhang, *Biosens. Bioelectron.*, 2008, **23**, 1117–1124.
8 P. Geng, X. Zhang, W. Meng, Q. Wang, W. Zhang, L. Jin, Z. Feng and Z. Wu, *Electrochim. Acta*, 2008, **53**, 4663–4668.
9 J.-G. Guan, Y.-Q. Miao and Q.-J. Zhang, *J. Biosci. Bioeng.*, 2004, **97**, 219–226.
10 R. Villalonga, M. L. Villalonga, P. Diez and J. M. Pingarron, *J. Mater. Chem.*, 2011, **21**, 12858–12864.
11 C.-S. Chen, K.-N. Chang, Y.-H. Chen, C.-K. Lee, B. Y.-J. Lee and A. S.-Y. Lee, *Biosens. Bioelectron.*, 2011, **26**, 3072–3076.
12 M. Labib, A. S. Zamay, D. Muharemagic, A. V. Chechik, J. C. Bell and M. V. Berezovski, *Anal. Chem.*, 2012, **84**, 1813–1816.
13 I. Willner and M. Zayats, *Angew. Chem., Int. Ed.*, 2007, **46**, 6408–6418.
14 I. Palchetti and M. Mascini, *Anal. Bioanal. Chem.*, 2012, **402**, 3103–3114.
15 B. J. Plowman, S. K. Bhargava and A. P. O'Mullane, *Analyst*, 2011, **136**, 5107–5119.

16 J. Wang, *Electroanalysis*, 2005, **17**, 7–14.
17 F. Xiao, Y. Li, X. Zan, K. Liao, R. Xu and H. Duan, *Adv. Funct. Mater.*, 2012, **22**, 2487–2494.
18 M. A. Lim, D. H. Kim, C.-O. Park, Y. W. Lee, S. W. Han, Z. Li, R. S. Williams and I. Park, *ACS Nano*, 2011, **6**, 598–608.
19 T.-M. Cheng, T.-K. Huang, H.-K. Lin, S.-P. Tung, Y.-L. Chen, C.-Y. Lee and H.-T. Chiu, *ACS Appl. Mater. Interfaces*, 2010, **2**, 2773–2780.
20 T.-K. Huang, Y.-C. Chen, H.-C. Ko, H.-W. Huang, C.-H. Wang, H.-K. Lin, F.-R. Chen, J.-J. Kai, C.-Y. Lee and H.-T. Chiu, *Langmuir*, 2008, **24**, 5647–5649.
21 Y.-C. Yang, T.-K. Huang, Y.-L. Chen, J.-Y. Mevellec, S. Lefrant, C.-Y. Lee and H.-T. Chiu, *J. Phys. Chem. C*, 2011, **115**, 1932–1939.
22 J. Bichler, J. A. Heit and W. G. Owen, *Thromb. Res.*, 1996, **84**, 289–294.
23 C. Lofton and W. Sigmund, *Adv. Funct. Mater.*, 2005, **15**, 1197–1208.
24 C. J. Murphy and N. R. Jana, *Adv. Mater.*, 2002, **14**, 80–82.
25 C. J. Johnson, E. Dujardin, S. A. Davis, C. J. Murphy and S. Mann, *J. Mater. Chem.*, 2002, **12**, 1765–1770.
26 Z.-Y. Jiang, Q. Kuang, Z.-X. Xie and L.-S. Zheng, *Adv. Funct. Mater.*, 2010, **20**, 3634–3645.
27 T. Herricks, J. Chen and Y. Xia, *Nano Lett.*, 2004, **4**, 2367–2371.
28 S. Trasatti and O. A. Petrii, *Pure Appl. Chem.*, 1991, **63**, 711–734.
29 L. C. Bock, L. C. Griffin, J. A. Latham, E. H. Vermaas and J. J. Toole, *Nature*, 1992, **355**, 564–566.
30 L. R. Paborsky, S. N. McCurdy, L. C. Griffin, J. J. Toole and L. L. K. Leung, *J. Biol. Chem.*, 1993, **268**, 20808–20811.
31 R. F. Macaya, P. Schultze, F. W. Smith, J. A. Roe and J. Feigon, *Proc. Natl. Acad. Sci. U. S. A.*, 1993, **90**, 3745.
32 B. I. Kankia and L. A. Marky, *J. Am. Chem. Soc.*, 2001, **123**, 10799–10804.
33 A. B. Steel, T. M. Herne and M. J. Tarlov, *Anal. Chem.*, 1998, **70**, 4670–4677.
34 J. S. Daniels and N. Pourmand, *Electroanalysis*, 2007, **19**, 1239–1257.
35 I. I. Suni, *TrAC, Trends Anal. Chem.*, 2008, **27**, 604–611.
36 F. Lisdat and D. Schäfer, *Anal. Bioanal. Chem.*, 2008, **391**, 1555–1567.
37 J. E. B. Randles, *Discuss. Faraday Soc.*, 1947, **1**, 11–19.
38 L. Li, H. Zhao, Z. Chen, X. Mu and L. Guo, *Anal. Bioanal. Chem.*, 2010, **398**, 563–570.
39 L. Bai, R. Yuan, Y. Chai, Y. Zhuo, Y. Yuan and Y. Wang, *Biomaterials*, 2012, **33**, 1090–1096.
40 D. Kwon, H. Jeong and B. H. Chung, *Biosens. Bioelectron.*, 2011, **28**, 454–458.
41 P. Kara, A. de la Escosura-Muñiz, M. Maltez-da Costa, M. Guix, M. Ozsoz and A. Merkoçi, *Biosens. Bioelectron.*, 2010, **26**, 1715–1718.
42 L.-D. Li, H.-T. Zhao, Z.-B. Chen, X.-J. Mu and L. Guo, *Sens. Actuators, B*, 2011, **157**, 189–194.
43 X. Li, L. Shen, D. Zhang, H. Qi, Q. Gao, F. Ma and C. Zhang, *Biosens. Bioelectron.*, 2008, **23**, 1624–1630.
44 A.-E. Radi, J. L. Acero. Sánchez, E. Baldrich and C. K. O'Sullivan, *Anal. Chem.*, 2005, **77**, 6320–6323.
45 Z. Zhang, W. Yang, J. Wang, C. Yang, F. Yang and X. Yang, *Talanta*, 2009, **78**, 1240–1245.
46 Y. Du, B. Li, H. Wei, Y. Wang and E. Wang, *Anal. Chem.*, 2008, **80**, 5110–5117.
47 C. Ocaña, M. Pacios and M. del Valle, *Sensors*, 2012, **12**, 3037–3048.